

# Numerical analysis using 2D modeling of optical fiber poled by induction

D. Huang<sup>1</sup>, F. De Lucia<sup>2</sup>, C. Corbari<sup>2</sup>, N. Healy<sup>2</sup> and P.J.A. Sazio<sup>2,\*</sup>

<sup>1</sup>Institute of High Performance Computing, Agency for Science, Technology, and Research (A\*STAR), 1 Fusionopolis Way, Singapore

<sup>2</sup>Optoelectronics Research Centre, University of Southampton, SO17 1BJ, UK

\*[pjas@soton.ac.uk](mailto:pjas@soton.ac.uk)

## ABSTRACT

Thermal poling, a technique to introduce effective second-order nonlinearities in silica optical fibers, has found widespread applications in frequency conversion, electro-optic modulation, switching and polarization-entangled photon pair generation. Since its first demonstration around 25 years ago, studies into thermal poling were primarily based on anode-cathode electrode configurations. However, more recently, superior electrode configurations have been investigated that allow for robust and reliable thermally poled fibers with excellent second order nonlinear properties [1, 2]. Very recently, we experimentally demonstrated an electrostatic induction poling technique that creates a stable second-order nonlinearity in a twin-hole fiber without any direct physical contact to internal fiber electrodes whatsoever [3]. This innovative technique lifts a number of restrictions on the use of complex microstructured optical fibers (MOF) for poling, as it is no longer necessary to individually contact internal electrodes and presents a general methodology for selective liquid electrode filling of complex MOF geometries. In order to systematically implement these more advanced device embodiments, it is first necessary to develop comprehensive numerical models of the induction poling mechanism itself. To this end, we have developed two-dimensional (2D) simulations of space-charge region formation using COMSOL finite element analysis, by building on current numerical models [4].

**Keywords:** nonlinear optics, numerical modeling, optical fibers

## 1. INTRODUCTION

The investigation of thermal poling, a technique to create effective second order nonlinearities in silica optical fibers [5], has allowed for a significant enlargement of the field of its applications such as for example parametric frequency conversion [6], electro-optic modulation, switching [7] and polarization-entangled photon pair generation [8]. The thermal poling process consists in heating up the optical fiber while a high voltage is applied for a certain time between two electrodes embedded into the fiber [9]. The method of poling described in [9], which can be defined as a conventional anode-cathode configuration, has the drawback of being characterized by a high risk of breakdown due to the small distance between the two electrodes (tens of  $\mu\text{m}$ ). This risk was mostly overcome by Margulis et al. [1], who developed a new method of poling that allowed for inducing a value of  $\chi_{eff}^{(2)}$  higher than the one obtained in the conventional case [9]. According to this new method the two embedded electrodes are both contacted to the same positive potential of the anode. This technique has been recently further developed by De Lucia et al. [3], who discovered that it is possible to induce a space charge region into a twin-hole fused silica fiber by means of a process of electrostatic induction between an inductor (a hollow-core fused silica fiber equipped with two tungsten electrodes both looped and connected to the same positive potential) and two floating electrodes embedded into a fused silica twin-hole fiber longer than the inductor. This new method negates the requirement of contact between the embedded electrodes and the HV supply, allowing for thermal poling of many different kinds of optical fibers when contacting the electrodes is a challenging issue. In this paper, we report a theoretical model based on 2D finite element analysis to explain the evolution of the electric equipotential surfaces in an induction poling experiment. The final aim of this work is to understand how the electrostatic induction mechanism drives the formation of a space charge region in a twin-hole silica fiber poled by induction and how the depletion region creation can be explained even in a point of the fiber far from the inductor.

## 2. THEORETICAL MODEL

### 2.1 Geometry of the model

The starting point of our work is the experimental observation of a depletion region (revealed by means of an HF etching process of the ends of a silica fiber) produced by poling a twin-hole silica fiber by induction and reported previously [3] in which we described the development of a numerical model (realized by means of COMSOL Multiphysics<sup>®</sup>) to simulate the initial electric potential distributions between the inductor, the sample, and the ground plane. The indirect electrostatic induction poling setup itself consists of two separate fibers with embedded electrodes, namely the “inductor” and the liquid metal-filled sample. The inductor is a multi-hole silica capillary 6 cm in length, outer diameter (OD) of 250  $\mu\text{m}$ , with two 25- $\mu\text{m}$ -diameter tungsten wires manually inserted inside. The sample is a twin-hole Germania doped fused silica fiber (length  $\approx 20$  cm, OD = 125  $\mu\text{m}$ ). The two holes of the sample were fully filled with metallic liquid electrodes by means of a pressure filling technique similar to the one described in [10]. The experimental setup of an induction poling experiment is reported in Fig.1. Fig. 2 shows the HF etched cross section of a fused silica sample poled by induction, while the initial 2D electric potential distribution (before poling begins) and a line scan through the geometric centers of the fibers are shown in Fig. 3.

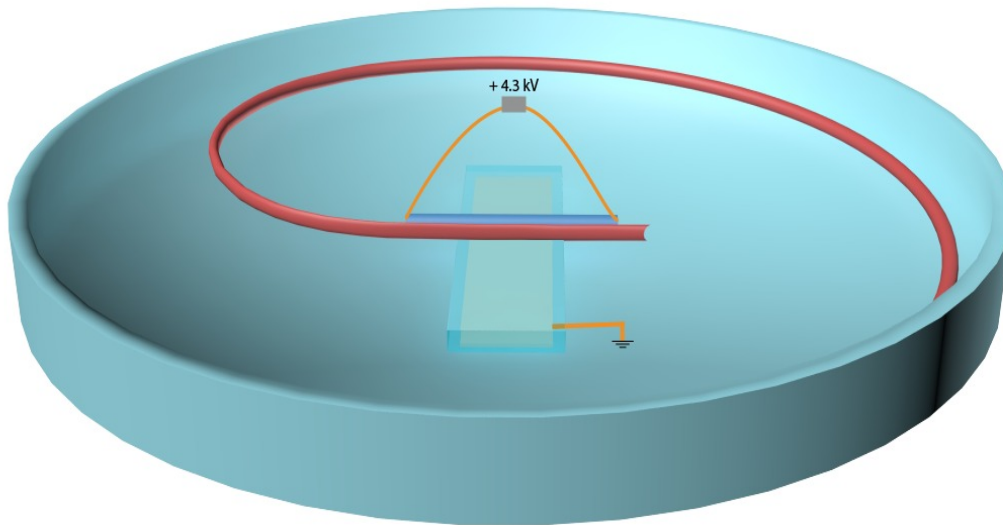


Figure 1. Electrostatic induction poling setup with inductor and sample in close proximity. The “inductor” is the blue fiber equipped with two tungsten wires connected to the anode. This fiber serves as a dielectric barrier to prevent unwanted electrical breakdown in air. The red fiber is the sample equipped with internal liquid metal electrodes. Both the inductor and sample are adhered to a borosilicate microscope slide that has a thin metallic layer evaporated onto its rear surface held at ground potential. At elevated temperatures the enhanced bulk conductivity of the glass slide allow it to act as a ground plane.

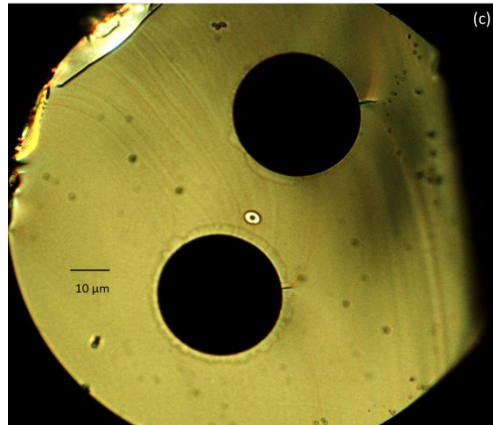


Fig. 2. Cross section of an Acreo Fiberlab twin-hole germania doped silica fiber poled by induction by means of the setup shown in Fig. 1. The experimental conditions of the poling experiments are: temperature of 300 °C, external voltage applied of 4.3 kV, duration of poling experiment of 100 minutes.

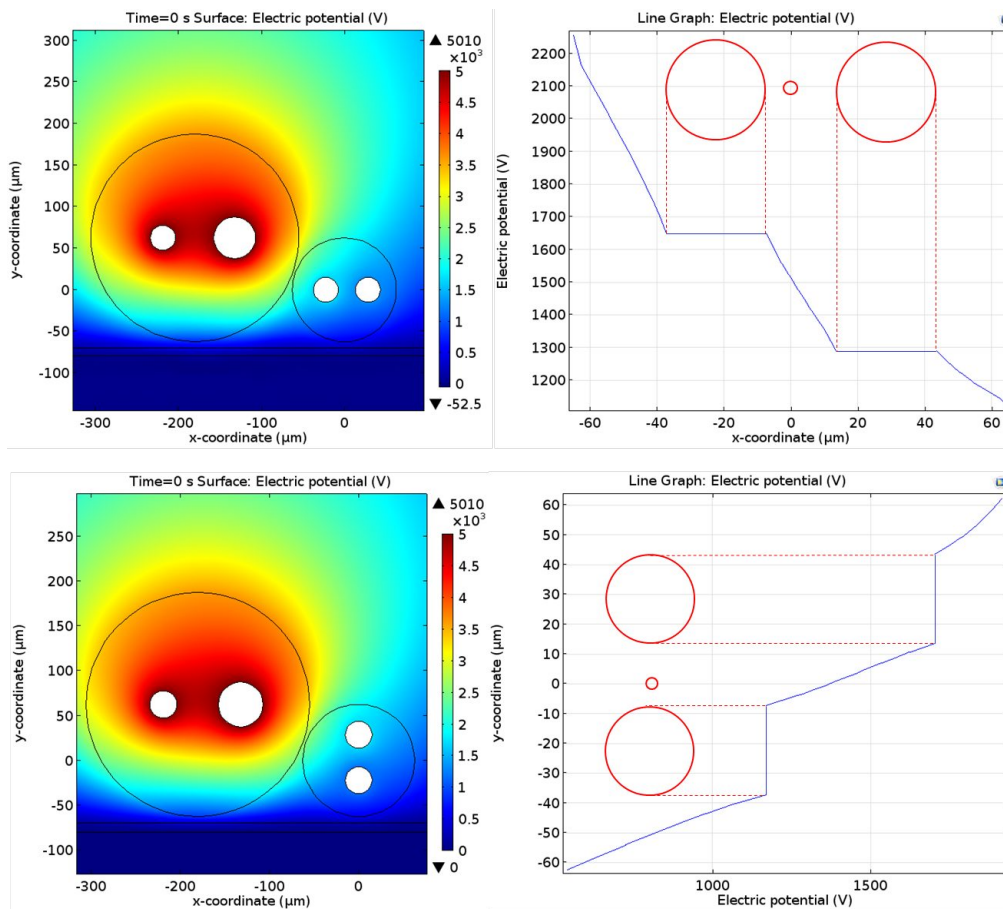


Figure 3. (Top-Left) Simulated initial 2D electric potential distribution calculated using Gauss' law before charged ion migration begins to generate the depletion region. The external inductor is the large diameter fiber structure, with the smaller diameter sample fiber located immediately adjacent to it. The model includes both grounded air box (a cube of side 10 cm) and incorporated ground plane. (Top-Right) A line scan through the geometric centers of the sample reveals large potential variations in the sample that can drive impurity ion migration for depletion formation in an induction poling experiment. (Bottom-Left) 2D electric potential distribution for a different orientation of the sample. (Bottom-Right) Line scan of the electric potential for the same orientation.

## 2.2 General equations

Fig. 3 shows the working principle of the induction poling method. Both the electrodes embedded into the sample, which is located near the inductor, pick up the electric potential electrostatically induced by the external electrodes connected to the anode and embedded into the multi-hole silica capillary. The potential difference between the two floating electrodes embedded in the sample causes the formation of the depletion region according an enhanced “avalanche-like” positive feedback mechanism similar to that described by Margulis et al. [1]. The origin of the depletion formation is the ionic migration inside the fiber. A sufficient number of cations (~1 ppm conc.) is required so that charge migration is substantial enough to produce a significant second-order nonlinearity. If both migration and diffusion are taken into account, the local equation of continuity and the Poisson's equation lead to the following system of partial differential equations:

$$\frac{\partial p_i}{\partial t} = -\mu_i \nabla(p_i E) + D_i \nabla^2(p_i) \quad (1)$$

$$\nabla E = \frac{e}{\varepsilon} [\sum_i (p_i - p_{0,i})] \quad (2)$$

where the index  $i$  represents a positively charged ionic species,  $p_i = p_i(x, y, t)$  is the instantaneous concentration of the  $i$ -th charge,  $\mu_i$  is its mobility,  $p_{0,i}$  denotes its initial concentration within the glass,  $e$  is the electronic charge, and  $\varepsilon = 2.09\varepsilon_0$  is the dielectric permittivity of silica glass.  $D_i$  is the diffusion constant, which is related to the mobility through the Nernst-Einstein relation  $D_i = k_B T \mu_i / e$ ,  $k_B$  being the Boltzmann's constant and  $T$  the temperature. The system of Eqs. (1) and (2) allows us to determine the spatial distribution of the electric field within the fiber from Gauss' law during ion migration. We can then in principle deduce the second-order nonlinearity spatial distribution within the fiber.

## 2.3 Model of induction poling near and far-from the inductor

The model developed to simulate the induction poling experiment, such as the one reported in Fig. 1, will include two sub-models. The first one (which can be defined as the model near the inductor), is characterized by the fact that the depletion region is driven by electrostatic induction developed between the externally applied electric potential and the two floating electrodes embedded into the sample. However, it is also necessary to consider the situation far from the inductor. In a position along the fiber located far from the inductor we can assume that the electrical behavior of the sample is not anymore characterized by the influence of the electric field lines produced by the external electric potential. In fact, we can assume that both the floating electrodes (in a point far from the inductor) will be characterized by an electric potential that is the one picked up by each of them in a position near the inductor. Moreover we assume that the electric potential picked up by each electrode evolves because of the temporal evolution of the induction poling process. In other words, the model to describe the induction poling experiment far from the inductor is exactly the one developed by Camara et al. [4], if we assume that the two electrodes embedded into the sample are ideal conductors in such a way that the potential in a point far from the inductor will be the same as the one captured in a point close to the inductor. Considering our model that describes the induction poling far from the inductor, the main difference with the model of [4] is that the ground is not located on the external surface of the fiber itself but, just like the model near the inductor, it is identified in the 10 x 10 x 10cm box walls and in the backplane of the borosilicate slide on top of which the fiber is placed. Fig. 4 shows the initial 2D distribution of the electric equipotential surfaces in a point of the fiber located far from the inductor.

## 2.4 Influence of orientation on the induction poling behavior

Our simulations also reveal that the relative azimuthal rotation angle of the sample with respect to the inductor can further modify the potential variation within the sample itself, thus demonstrating that induction poling can be engineered and optimized with many different parameters. For example, in comparing the relative orientations of the inductor and the sample, the initial electric potential difference between the two floating electrodes of the sample is bigger in the case of an orthogonal relative orientation than in the case of the same orientation (see Fig. 3 Top-Right and Bottom-Right). In terms of space charge region formation this means that the dynamics of the process will be faster in the case of orthogonal orientation than in the case of same orientation, producing in this way a larger depletion region if

considered for a certain time. In a position located far from the inductor (see Fig. 4) the electric potential difference between the two floating electrodes is characterized by the same behavior as near the inductor with the only difference being that the process of creation of the space charge region will not be influenced by the presence of the inductor and so will result in a homogeneous development of both the depletion regions around the two electrodes.

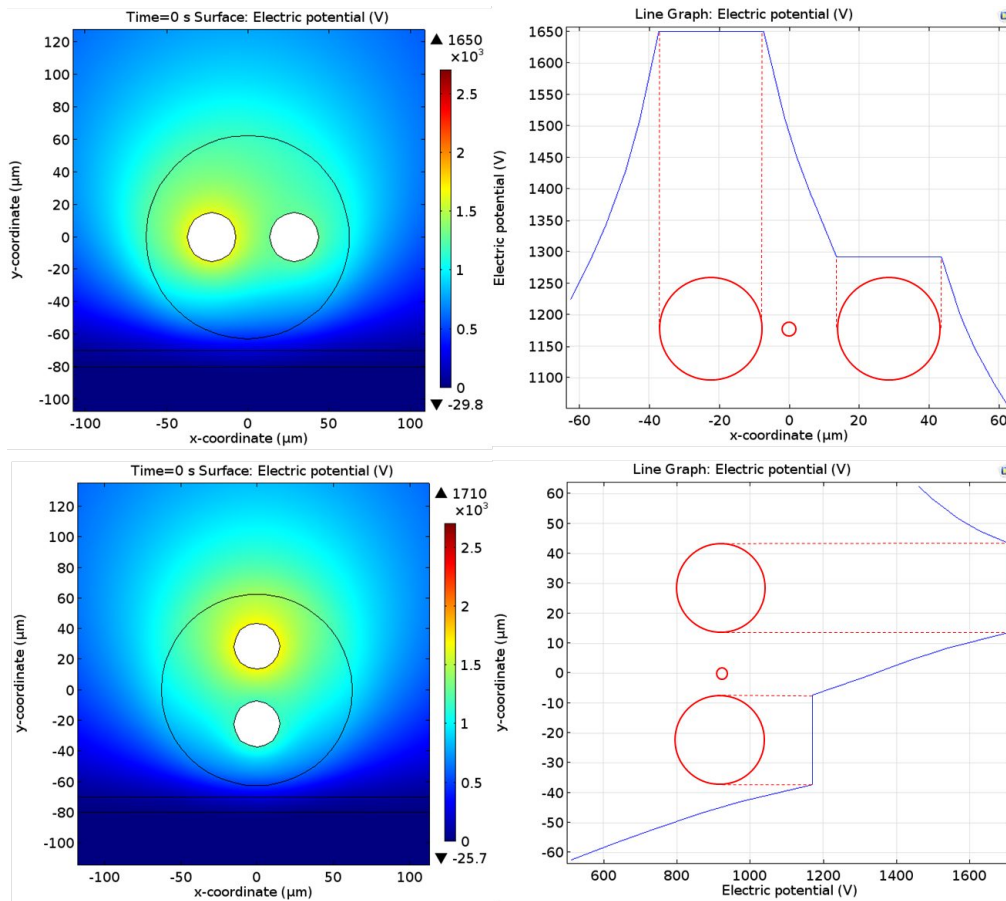


Figure 4. (Top-Left) Simulated initial 2D electric potential distribution for a section of the sample located in a position far from the inductor. The model includes both grounded air box (cube of side 10 cm) and incorporated ground plane. (Top-Right) A line scan through the geometric centers of the sample reveals large potential variations in the sample that can drive impurity ion migration for depletion formation in an induction poling experiment. (Bottom-Left) 2D electric potential distribution for a different orientation of the sample. (Bottom-Right) Line scan of the electric potential for the same orientation.

### 3. CONCLUSION

We presented the results of a 2D numerical simulation developed using COMSOL Multiphysics<sup>®</sup> to explain the evolution of the electric equipotentials for an electrostatic induction poling experiment of a silica fiber embedded with two floating electrodes. The simulations confirm that the floating electrodes pick up the electric potential created by the electrodes connected to the anode and embedded into the inductor fiber to allow for the creation of a space charge region which can subsequently induce a second order nonlinearity into the fiber. The electrical continuity of the electrodes, if the fiber is held at the correct poling temperature, will allow for the creation of a depletion region even in regions of the fiber located far from the inductor. In fact, this distance can be orders of magnitude longer than the length of the inductor itself [3]. The most relevant difference which distinguishes the model near the inductor with respect to the one that describes the situation far from the inductor concerns the presence of the electric field lines which modify the dynamics of the depletion region formation in the two different positions.

#### 4. ACKNOWLEDGMENTS

The authors acknowledge EPSRC EP/I035307/1 for financial support. The authors would like to thank Oleksandr Tarasenko and Walter Margulis from Acreo Fiberlab who manufactured the fiber used for induction poling experiments and Peter Kazansky at the Optoelectronics Research Centre of the University of Southampton for access to the necessary technical facilities. Datasets for figures included in this paper available at <http://dx.doi.org/10.5258/SOTON/386020>

#### REFERENCES

- [1] Margulis, M., Tarasenko, O. and Myren, N., "Who needs a cathode? Creating a second-order nonlinearity by charging glass fiber with two anodes," *Opt. Exp.* 17(18), 15534-15540 (2009).
- [2] An, H. and Fleming, S., "Investigating the effectiveness of thermally poling optical fibres with various internal electrode configurations," *Opt. Exp.* 20(7), 7436-7444 (2012).
- [3] De Lucia, F., Huang, D., Corbari, C., Healy, N. and Sazio, P. J. A., "Optical fiber poling by induction," *Opt. Lett.* 39(22), 6513-6516 (2014).
- [4] Camara, A., Tarasenko, O. and Margulis, W., "Study of thermally poled fibers with a two-dimensional model," *Opt. Exp.* 22(15), 17700-17715 (2014).
- [5] Myers, R. A., Mukherjee, N. and Brueck, S. R. J., "Large second-order nonlinearity in poled fused silica," *Opt. Lett.* 16(22), 1732-1734 (1991).
- [6] Canagasabey, A., Corbari, C., Gladyshev, A. V., Liegeois, F., Guillemet, S., Hernandez, Y., Yashkov, M. V., Kosolapov, A., Dianov, E. M., Ibsen, M. and Kazansky, P. G., "High-average-power second-harmonic generation from periodically poled silica fibers," *Opt. Lett.* 34(16), 2483-2485 (2009).
- [7] Malmstrom, M., Tarasenko, O. and Margulis, M., "Pulse selection at 1 MHz with electrooptic fiber switch," *Opt. Exp.* 20(9), 9465-9470 (2012).
- [8] Zhu, E. Y., Tang, Z., Qian, L., Helt, L. G., Liscidini, M., JSipe, J. E., Corbari, C., Canagasabey, A., Ibsen, M. and P. G. Kazansky, "Poled-fiber source of broadband polarization-entangled photon pairs," *Opt. Lett.* 38(21), 4397-4400 (2013).
- [9] Wong, D., Xu, W., Fleming, S., Janos, M. and Lo, K-M, "Frozen-in electrical field in thermally poled fibers," *Opt. Fib. Tech.* 5, 235-241 (1999).
- [10] Fokine, M., Nilsson, L. E., Claesson, A. A., Berlemont, D., Kjellberg, D., Krummenacher, L. and Margulis, W., "Integrated fiber Mach-Zehnder interferometer for electro-optic switching," *Opt. Lett.* 27(18), 1643-1645 (2002).